BMC Medical Imaging

RESEARCH

Open Access

Computed tomography enterography-based radiomics nomograms to predict inflammatory activity for ileocolonic Crohn's disease: a preliminary single-center retrospective study

Yuping Ma[1†], Luanxin Zhu[2†], Bota Cui[3], Faming Zhang[3], Haige Li[1] and Jianguo Zhu[1*]

Abstract

Objectives This study aims to develop and validate nomograms that utilize morphological and radiomics features derived from computed tomography enterography (CTE) to evaluate inflammatory activity in patients with ileocolonic Crohn's disease (CD).

Methods A total of 54 CD patients (237 bowel segments) with clinically confirmed CD were retrospectively analyzed. The Simple Endoscopic Score for Crohn's Disease (SES-CD) was used as a reference standard to quantify the degree of mucosal inflammation and assess disease severity. We extracted morphological and radiomics features in the training cohort to create a morphological model (M-score) and a radiomics model (Rad-score). A combined nomogram was generated by integrating the M-score and Rad-score. The predictive performance of each model was evaluated using receiver operating characteristic (ROC) curve analysis. Additionally, calibration curve and decision curve analysis (DCA) were employed to assess the accuracy and clinical applicability of the nomogram in the testing cohort.

Results The area under the ROC curve (AUC) for the nomogram, which included stenosis, comb sign, and Rad-score, was 0.834 [95% confidence interval (CI): 0.728–0.940] for distinguishing between active and remissive disease. Furthermore, the nomogram created using comb sign and Rad-score achieved a satisfactory AUC of 0.781 (95% CI: 0.611–0.951) in differentiating mild activity from moderate-to-severe activity. The calibration curve and DCA confirmed both nomograms' accuracy and clinical utility.

Conclusions Nomograms that combined CTE-based radiomics and morphological features could serve as valuable tools for assessing inflammatory activity, thereby supporting clinical decision-making in managing CD. Keypoints. 1. Radiomics features from CTE could predict the inflammatory activity of CD.

Keypoints

1. Radiomics features from CTE could predict the inflammatory activity of CD.
2. The nomograms were most effective in predicting inflammatory activity.
3. Radiomics enhanced radiologists' ability to evaluate inflammatory activity.

†Yuping Ma and Luanxin Zhu contributed equally to this work.

*Correspondence:
Jianguo Zhu
zhujianguo@njmu.edu.cn
Full list of author information is available at the end of the article

Keywords Crohn's disease, Computed tomography enterography, Radiomics, Inflammatory activity

Introduction

Crohn's disease (CD) is a chronic, relapsing inflammatory disease affecting the entire gastrointestinal tract. If not properly managed, it can significantly impact patients' quality of life and lead to various complications [1]. Therefore, accurately and efficiently assessing disease activity is essential for the monitoring and management of CD [2].

Several well-established scoring criteria existed for evaluating disease activity in CD, including Crohn's disease activity index (CDAI) and Harvey-Bradshaw index (HBI) based on symptoms and physical signs, Crohn's disease endoscopic index of severity and Simple Endoscopic Score for Crohn's Disease (SES-CD) which are based on endoscopic findings, magnetic resonance index of activity (MaRIA), Clermont score and magnetic resonance enterography global score (MEGS) using magnetic resonance enterography [3–6]. Among these, endoscopic scoring is commonly used and is considered as the reference standard in many studies. However, endoscopic procedures have limitations, e.g., invasive, costly, and accompanied by risks of complications [7, 8]. Computed tomography enterography (CTE) and magnetic resonance enterography (MRE) are frequently used to diagnose and evaluate CD in clinical works [9]. Compared with MRE, CTE demonstrates similar specificity and sensitivity in diagnosing CD [10], while also offering greater feasibility due to shorter imaging time, higher spatial and temporal resolution, fewer artifacts, and lower cost [11]. Radiomics, a well-recognized method for extracting quantitative parameters from medical images at a large scale, can illustrate hidden tissue heterogeneity and has been recently proposed as a promising tool to facilitate the transition to personalized medicine in clinical practice [12]. A few studies have indicated that radiomics model based on MRI data predicted CD diagnosis with better performance than MaRIA evaluated by senior radiologists [13, 14]. Moreover, other researches have focused on using radiomics signatures from mesenteric and intestinal CTE to predict the therapeutic response, postoperative anastomotic recurrence, fibrosis, and disease progression [11, 13, 15–19]. These results showed that radiomics were more accurate than relying solely on clinical factors or evaluations by senior radiologists. However, there are no validated CD activity scores derived from CTE data currently. Therefore, it is crucial to develop a reliable, objective method to identify CTE lesions in CD patients and assess disease activity.

In this study, we aimed to establish and validate nomograms to predict CD activity by integrating CTE-based radiomics with morphological features.

Materials and methods

Patient selection

This retrospective study was approved by the institutional review board of our hospital (approval number: 2013KY034), and written informed consent from each participant was waived.

We searched the radiology reports for the term Crohn's disease on CTE scans obtained between January 2017 and June 2023. The inclusion criteria for participants were as follows: (1) a confirmed diagnosis of CD based on conventional clinical, endoscopic, and histological criteria, (2) undergoing ileocolonoscopy within two days following the CTE, and (3) not having received any new medication between the 2 examinations. The exclusion criteria included: (1) inadequate imaging quality which was unable to segment, such as breathing artifact, (2) unclear intestinal contour on CTE due to severe perienteric effusion, intestinal adhesion, or peristalsis. Enrolled segments were randomly divided into a training cohort and a testing cohort at a ratio of 7:3. The study flow diagram is shown in Fig. 1. The following baseline data were collected: age, sex, disease duration, Montreal location, C-reactive protein level (CRP), erythrocyte sedimentation rate (ESR), HBI, SES-CD total score of each patient, and the features of each bowel segment.

Reference standard for intestinal inflammatory activity

The ileocolonoscopic procedure and evaluation were conducted by two gastroenterologists (with 15- and 20-years work experience, respectively) without knowledge of CTE results. The ileocolon was divided into 5 segments on ileocolonoscopy and CTE including the terminal ileum (the last 20 cm of small bowel proximal to the ileocecal valve), right colon (ileocecal valve, cecum, and ascending colon), transverse colon, left colon (descending and sigmoid colon), and rectum [15]. The gastroenterologists assessed and scored the ileocolonoscopic findings for each segment according to SES-CD during endoscopy. Inflammatory activity was classified by SES-CD as: inactive (0–2), mild (3–6), or moderate-severe ($\geq$7) [15]. Discrepancies between reviewers were resolved by consensus reading. The final results were used for further statistical analyses.

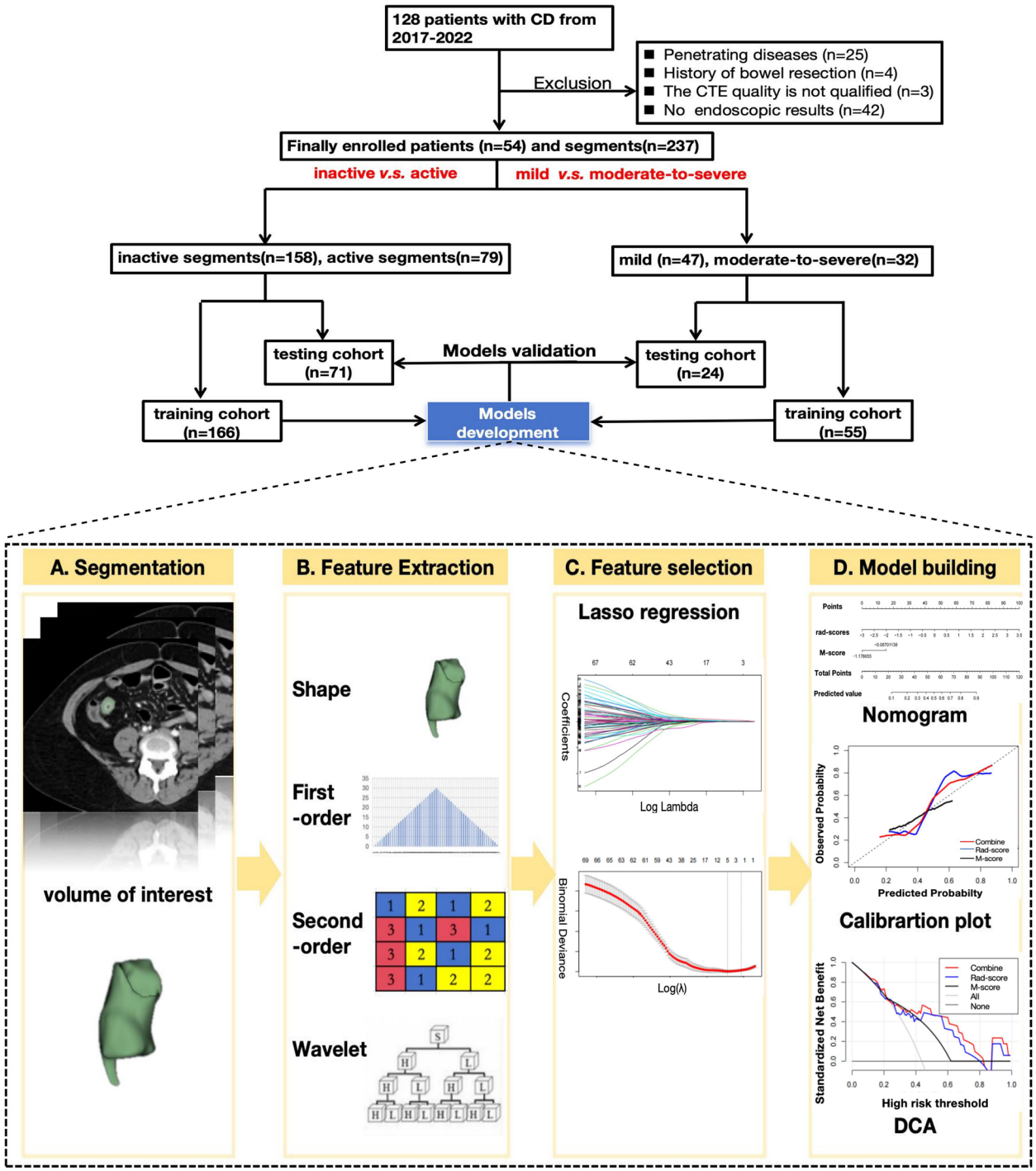

Fig. 1 Flow diagram of the study population and radiomics workflow Note: CD = Crohn's disease, LASSO = least absolute shrinkage and selection, DCA = decision curve analysis

Computed tomography enterography examination and CT morphological features by radiologist

CTE imaging technique

CTE examinations were performed using a dual-source dual-energy CT scanner (Somatom Definition, Siemens Healthineers, Forchheim GER) with tube current modulation (Care-Dose 4D), tube voltages of 100 kVp (A tube) and Sn-filtered 140 kVp (B tube). All subjects were scanned in a supine position. Fasting for solid food with a time interval of 8 h before the CTE scan was requested

for each subject. Additionally, all subjects needed to drink 300 mL of mannitol (2.5%) every 15 min until a total of 1.5 L had been consumed within 60 min. Intravenous contrast (Ultravist, Bayer, GA) was administered at a rate of 3 mL/s. Images at the axial direction with a slice thickness of 1 mm from the diaphragm to the pubic symphysis were acquired and sent to the picture archiving and communication system (PACS) (Carestream Health, Inc., Rochester, US). The CTE acquisition included the venous phase at 60 s after contrast administration.

CTE morphological analysis and model construction

There were five qualitative morphological features obtained by evaluating CTE:

(1) Bowel Wall Thickness: This feature is graded based on the thickness of the bowel wall as follows:

- Score 0: less than 3 mm.
- Score 1: mild thickness (3–5 mm).
- Score 2: moderate thickness (5–10 mm).
- Score 3: severe thickness (more than 10 mm).

(2) Lumen Stenosis: It is characterized by a reduction of 50% or more in luminal diameter compared with an adjacent loop, together with unequivocal upstream dilation of the same loop (>3 cm in caliber) [15]. It is graded as:

- Score 0: None.
- Score 1: Present.

(3) Mural Enhancement [15]:

- Score 0: Homogenous.
- Score 1: Asymmetric.
- Score 2: Stratified.

(4) Comb Sign is defined as segmental dilatation of the vasa recta involving a bowel loop [15]:

- Score 0: None.
- Score 1: Present.

(5) Fat Infiltration is defined as local and increased inhomogeneous attenuation in the perienteric fat, compared with the perienteric fat adjacent to non-inflamed bowel loops [15]:

- Score 0: None.
- Score 1: Present.

A radiologist with 20 years of experience in abdominal CT, blinded to the endoscopic results, evaluated these five features and scored. These five morphological features served as inputs for the multiple logistic regression analysis, and then a morphological model (M-score) was built.

Bowel segmentation and radiomics features extraction

Figure 1 illustrated the flow chart of our study. CTE venous phase images were used for lesion extraction. Volumes of interest (VOIs) were outlined along the contour of each lesion on each transverse section until the full lesion was captured excluding the intestinal lumen. A radiologist (reader 1, with 5 years of diagnostic experience in abdominal imaging) manually delineated three-dimensional (3D) VOIs using an open-source medical imaging software (3D-Slicer, version 5.5.0, https://www.slicer.org) and was blinded to the results of ileocolonoscopy.

To standardize the voxel spacing across the cohort, all CT voxels were resampled to a dimension of $1 \times 1 \times 1 mm^3$ before feature extraction. A fixed bin width of 25 Hounsfield units (HU) was used during the calculation of texture features. A total of 851 radiomics features were extracted, including shape, first-order, second-order, and wavelet-filter features.

To evaluate the inter- and intra-observer reproducibility of the extracted features, 30 segments randomly selected from the training cohort were segmented twice over a 4-week interval by another radiologist (reader 2, with 5 years of working experience in abdominal imaging) with the same procedures. The intraclass correlation coefficients (ICCs) were calculated using a two-way random effects model to determine inter- and intra-observer reliability. Only the features with an ICC of more than 0.75 were included in further analysis.

Radiomics model and morphological radiomics nomogram construction

Firstly, a pair-wise correlation analysis was performed to remove redundant radiomics features using the "findCorrelation" function from the R package "caret", with the absolute correlation cutoff set at 0.9. Then, least absolute shrinkage and selection (LASSO) logistic regression was adopted to select the most predictive radiomics features from the training cohort [20]. The penalty parameter lambda determining feature selection was chosen by 10-fold cross-validation. Next, a radiomics signature score (Rad-score) was constructed with a linear combination of selected features weighted by their respective coefficients. Finally, a nomogram by combining the M-score and the Rad-score with logistic regression was constructed.

Statistical analysis

Continuous variables were presented as the mean ± standard deviation when it followed a normal distribution; otherwise, they were presented as the median (P25, P75). All categorical variables were summarized as numbers (percent) and compared using Fisher's exact test. The diagnostic performance of the morphological model, the radiomics model, and the nomogram was evaluated using the area under the receiver operating characteristic (ROC) curve in both the training and testing cohorts. Delong method was employed to test the difference of the area under the ROC curves (AUC) among three models. Calibration curves were applied to evaluate the performance of the nomogram. Decision curve analysis (DCA) was conducted to evaluate the clinical efficacy of the nomogram by quantifying the net benefit at different threshold probabilities across the training and testing cohorts. Statistical analysis was performed using R software (version 4.3.1, www.r-project.org) with packages *caret*, *glmnet*, *pROC*, *reportROC*, *rms*, *rmda*, and *survival*. A two-sided $P<0.05$ was considered significant.

Results

Patient characteristics

A total of 54 patients with 237 bowel segments were included in the study. According to the SES-CD, 237 ileocolonic segments with CD lesions were classified as: inactive ($n=158$), mild ($n=47$), and moderate to severe ($n=32$). The clinical features of patients were showed in Table 1. The stratified distributions of SES-CD scores were compared between the training and testing cohorts (Table 2). 166 segments in the training cohort and 71 segments in the testing cohort were applied to differentiate active from remissive disease, while 55 in the training cohort and 24 in the testing cohort were used to distinguish mild from moderate-to-severe active disease.

Table 1 Clinical factors of patients

Clinical factors	Statistics analysis
Age at CD diagnosis (year) (mean ± SD)	40 ± 12.1
Gender, n (%)	
Female	19 (35.1)
Male	35(64.8)
Disease duration (years), median (IQR)	9 (5, 10)
Montreal location, n (%)	
Ileal (L1)	5 (9.2)
Colonic (L2)	31 (57.4)
Ileocolonic (L3)	18 (33.3)
CRP (mg/dL), median (IQR)	3.3 (0.5, 14.8)
ESR (mm/h), median (IQR)	16 (5, 32)
HBI, median (IQR)	5 (2, 9)
Total SES-CD, median (IQR)	6 (3, 12)

CRP C-reactive protein level, *ESR* erythrocyte sedimentation rate, *HBI* Harvey-Bradshaw, *SES-CD* simple endoscopic score for Crohn's disease, *IQR* interquartile range, *SD* standard deviation

Development and validation of models and nomogram for discriminating inactive from active bowel segments

Morphological features selection and M-score1 development

Bowel stenosis and comb sign were significantly associated with the activity of segments ($P<0.05$). These two morphological features were included to build M-score1: $-2.197+3.960\times$stenosis $+3.407\times$comb sign. The AUC was 0.870 (95% CI: 0.810–0.930) in the training cohort and 0.747 (95% CI: 0.638–0.855) in the testing cohort (Table 3).

Radiomics features selection and Rad-score1 development

A total of 830 features with inter- and intra-observer ICCs of ≥0.75 were retained as factors for developing the radiomics model. Further reduction of pair-wise correlations led to 494 independent features. After LASSO logistic regression from the training cohort (Fig. 2), three radiomics features with non-zero coefficients were selected to distinguish inactive from active segments. The Rad-score1 (inactive vs. active) was calculated by the following formula: $-0.8875+0.9790\times$wavelet-LLL-firstorder-Energy $+0.6177\times$wavelet-HLL-glszm-SizeZoneNonUniformity $+0.6542\times$original-firstorder-Median. The AUC for this model was 0.857 (95% CI: 0.797–0.918) in the training cohort and 0.828 (95% CI: 0.720–0.917) in the testing cohort (Table 3).

Although M-score1 outperformed Rad-score1 in differentiating activities in the training cohort, the Delong test revealed no significant difference between the two models ($P>0.05$).

Development and validation of combine-model1 and nomogram

We combined the M-score1 and Rad-score1 to construct the combine-model1: $0.4841+0.7422\times$M-score1 $+0.8732\times$Rad-score1. The prediction performance of combine-model1 achieved the optimal efficacy in bowel segments with an AUC, accuracy, sensibility, and specificity of 0.834 (95% CI: 0.728–0.940), 0.803, 0.692, 0.867 in the testing cohort respectively (Table 3). In both training and testing cohorts, the AUC of combine-model1 performed better than M-score1 ($P<0.05$) (Table 5). A nomogram based on the combine-model1 was built to visualize the results (Fig. 2). The calibration curve of the nomogram indicated good predictive accuracy between the actual and predicted probability. The DCA demonstrated a highly positive net benefit of the nomogram within a certain range (Fig. 3).

Table 2 Comparison of clinical data between training and testing cohort

	Active vs. inactive		Mild vs. moderate-to-severe	
	Training cohort *n* = 166	**Testing cohort *n* = 71**	**Training cohort *n* = 55**	**Testing cohort *n* = 24**
Segments with SES-CD score available, n (%)	*P* = 0.988		*P* = 0.689	
Terminal ileum	25 (15.1)	12 (16.9)	11 (20.0)	6 (25.0)
Right colon	33 (19.9)	14 (19.7)	17 (30.9)	8 (33.3)
Transverse colon	32 (19.3)	15 (21.1)	7 (12.7)	2 (8.3)
Left colon	38 (22.9)	15 (21.1)	13 (23.6)	3 (12.5)
Rectum	38 (22.9)	15 (21.1)	7 (12.7)	5 (20.8)
Morphology features				
Bowel wall thickness, n (%)	*P* = 0.462		*P* = 0.566	
0	62 (37.3)	25 (35.2)	1 (1.8)	1 (4.2)
1	48 (28.9)	21 (29.6)	7 (12.7)	4 (16.7)
2	30 (18.1)	18 (25.4)	22 (40.0)	12 (50.0)
3	26 (15.7)	7 (9.9)	25 (45.5)	7 (29.2)
Lumen stenosis	*P* = 0.289		*P* = 0.941	
0	133 (80.1)	61 (85.9)	28 (50.9)	12 (50.0)
1	33 (19.9)	10 (14.1)	27 (49.1)	12 (50.0)
Mural enhancement	*P* = 0.738		*P* = 0.632	
0	114 (68.7)	50 (70.4)	16 (29.1)	9 (37.5)
1	51 (30.7)	20 (28.2)	38 (69.1)	15 (62.5)
2	1 (0.06)	1 (1.4)	1 (1.8)	0 (0)
Comb sign	*P* = 0.030		*P* = 0.975	
0	124 (74.7)	53 (74.6)	25 (45.5)	11 (45.8)
1	42 (25.3)	18 (25.4)	30 (54.5)	13 (54.2)
Fat infiltration	*P* = 0.267		*P* = 0.128	
0	102 (61.4)	49 (69.0)	8 (14.5)	7 (29.2)
1	64 (38.6)	22 (31.0)	47 (85.5)	17 (70.8)
SES-CD, n (%)	*P* = 0.160		*P* = 0.719	
Inactive (0–2)	106 (63.9)	52 (73.2)		
Mild (3–6)	60 (36.1)	19 (26.8)	32 (58.2)	15 (62.5)
Moderate-to-severe (≥ 7)			23 (41.8)	9 (37.5)

SES-CD simple endoscopic score for Crohn's disease

Table 3 Performance of models for differentiating active from inactive disease

models	Training cohort				Testing cohort			
	AUC (95%CI)	**Accuracy**	**Sensitivity**	**Specificity**	**AUC (95%CI)**	**Accuracy**	**Sensitivity**	**Specificity**
M-score1	0.870(0.810–0.930)	0.892	0.774	0.947	0.747(0.638–0.855)	0.775	0.577	0.889
Rad-score1	0.857(0.797–0.918)	0.771	0.830	0.743	0.828(0.720–0.937)	0.789	0.769	0.800
Combine-model1	0.944(0.905–0.982)	0.916	0.868	0.938	0.834(0.728–0.940)	0.803	0.692	0.867

Development and validation of models and nomogram for discriminating mild active from moderate-to-severe active bowel segments

Construction of three models

We used the same modeling process previously described to distinguish mild active from moderate-to-severe active bowel segments. The M-score2 (mild vs. moderate-to-severe) was calculated as follows: $-1.1787 + 1.0916 \times$comb sign. One radiomics feature was included in Rad-score 2: $-1.2670 + 1.3048 \times$wavelet-HLL-glszm-SizeZoneNonUniformity. Subsequently, the combine-model2 was constructed with the combination of the M-score2 and the Rad-model2

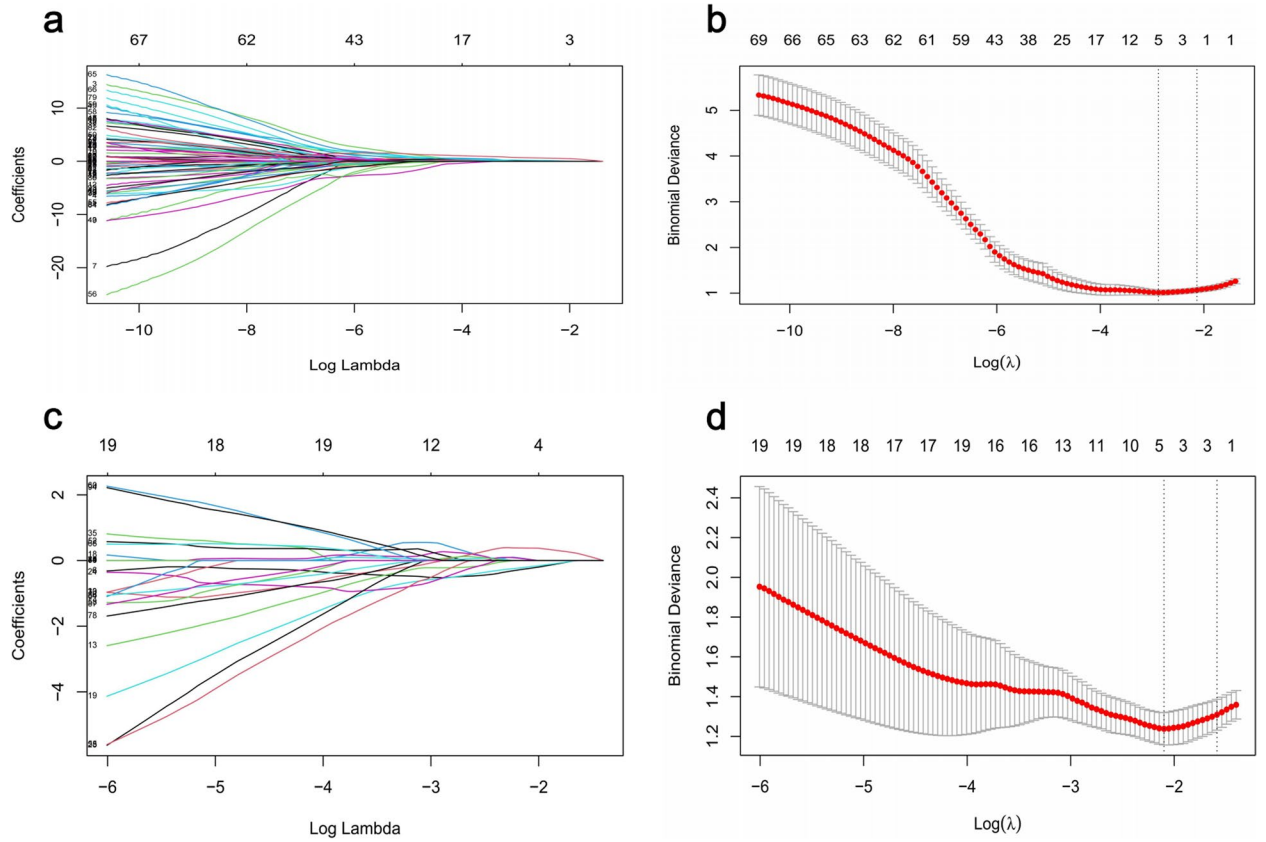

Fig. 2 Screening of variables based on Lasso regression (**a**) and (**b**) are Lasso regression for predicting active and inactive disease, (**c**) and (**d**) are for mild and moderate-to-moderate activity. **a** and **c** are the variation characteristics of the coefficients of variables; (**b**) and (**d**) are the selection process of the optimum value of the parameter λ in the Lasso regression model by the 10-fold cross-validation method

as follows: −1.9143 + 1.0340×M-score2 + 1.3627×Rad-score2. The nomogram for differentiating mild activity from moderate to severe activity was plotted based on the combine-model2 (Fig. 4).

Performance comparison

Table 4 summarized the AUC, accuracy, sensibility, and specificity. The combine-model2 showed a favorable performance with an AUC of 0.817 (95% CI: 0.676–0.958) in the training cohort and 0.781 (95% CI: 0.611–0.951) in the testing cohort. Moreover, the Delong test revealed that the difference was statistically significant between combine-model2 and both M-model2 and Rad-score2 (both, $P < 0.05$, Table 5).

Calibration and clinical utility of models

Calibration plots and DCA of three models in the testing cohort for distinguishing mild activity from moderate-to-severe activity were shown in Fig. 4.

Discussion

We used CTE images to develop and validate a radiomics-based nomogram for identifying the activity of CD lesions. Our study demonstrated that in both the training and testing cohorts, the nomogram which combined imaging morphological features and radiomics features could accurately distinguish the severity of disease activity. It performed better than either a single radiomics model or evaluations made by a senior radiologist.

The CD has a variable clinical course, characterized by alternating periods of activity and remission [15]. Hence, it is essential to accurately and promptly assess the activity of CD, which can help clinicians in selecting appropriate treatments. The SES-CD score is the most reliable scoring tool for CD [21]. However, failure to intubate the ileum is a major challenge when using the SES-CD as a primary outcome in clinical trials [22]. CTE is an imaging method that can evaluate not only the whole gastrointestinal tract involvement but also the extra-intestinal complications noninvasively.

Our study focused on investigating the morphological features associated with CD. Multi-logistic analysis

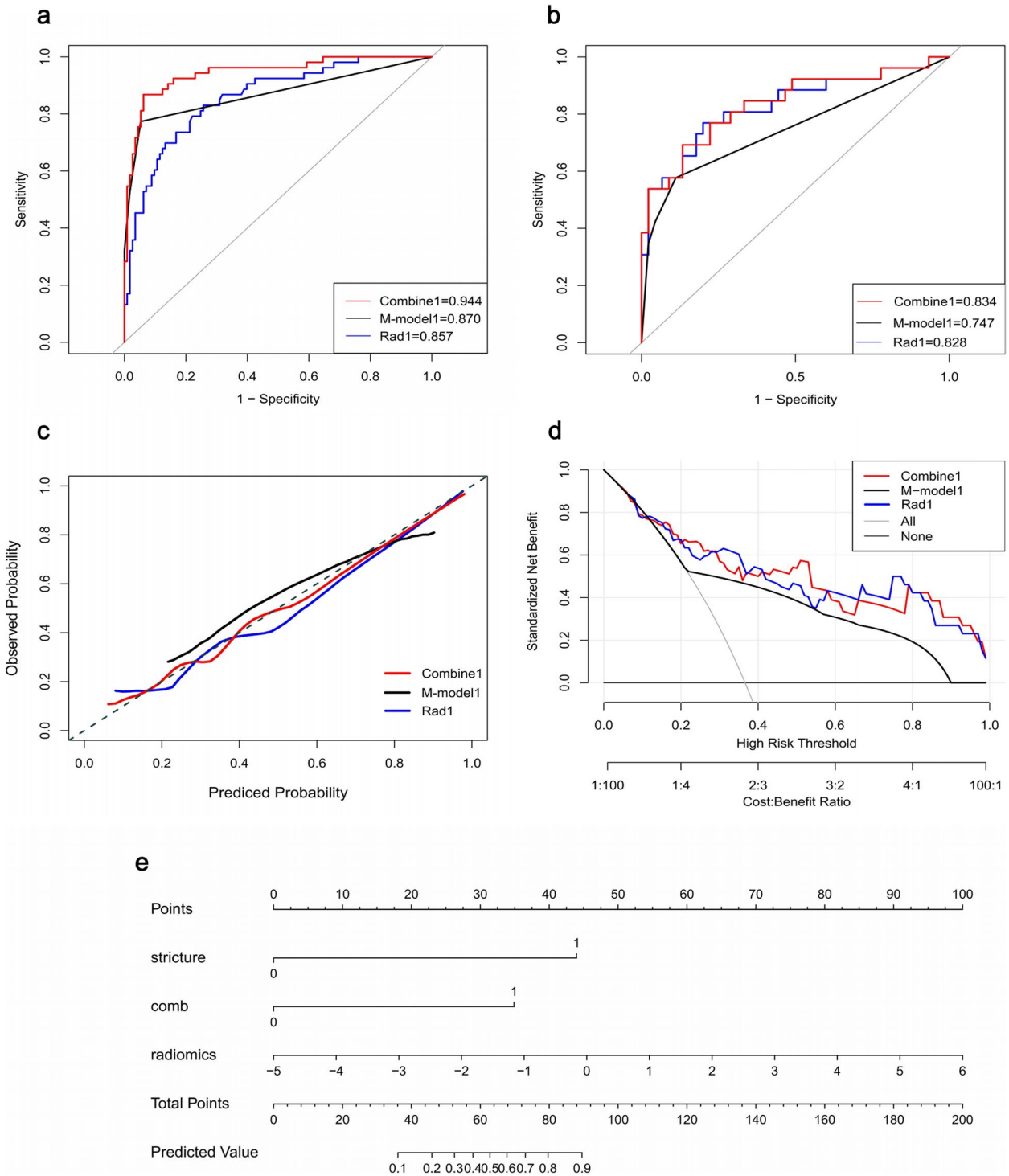

Fig. 3 The output of three models in distinguishing active from inactive disease (**a**-**b**) ROC of combine-model, radiomics-model, and morphology model in the training and testing cohort. **c** Calibration of three models in the testing cohort. **d** Decision curve analysis (DCA) of three models in the testing cohort. **e** Nomogram constructed by morphology radiomics combined model

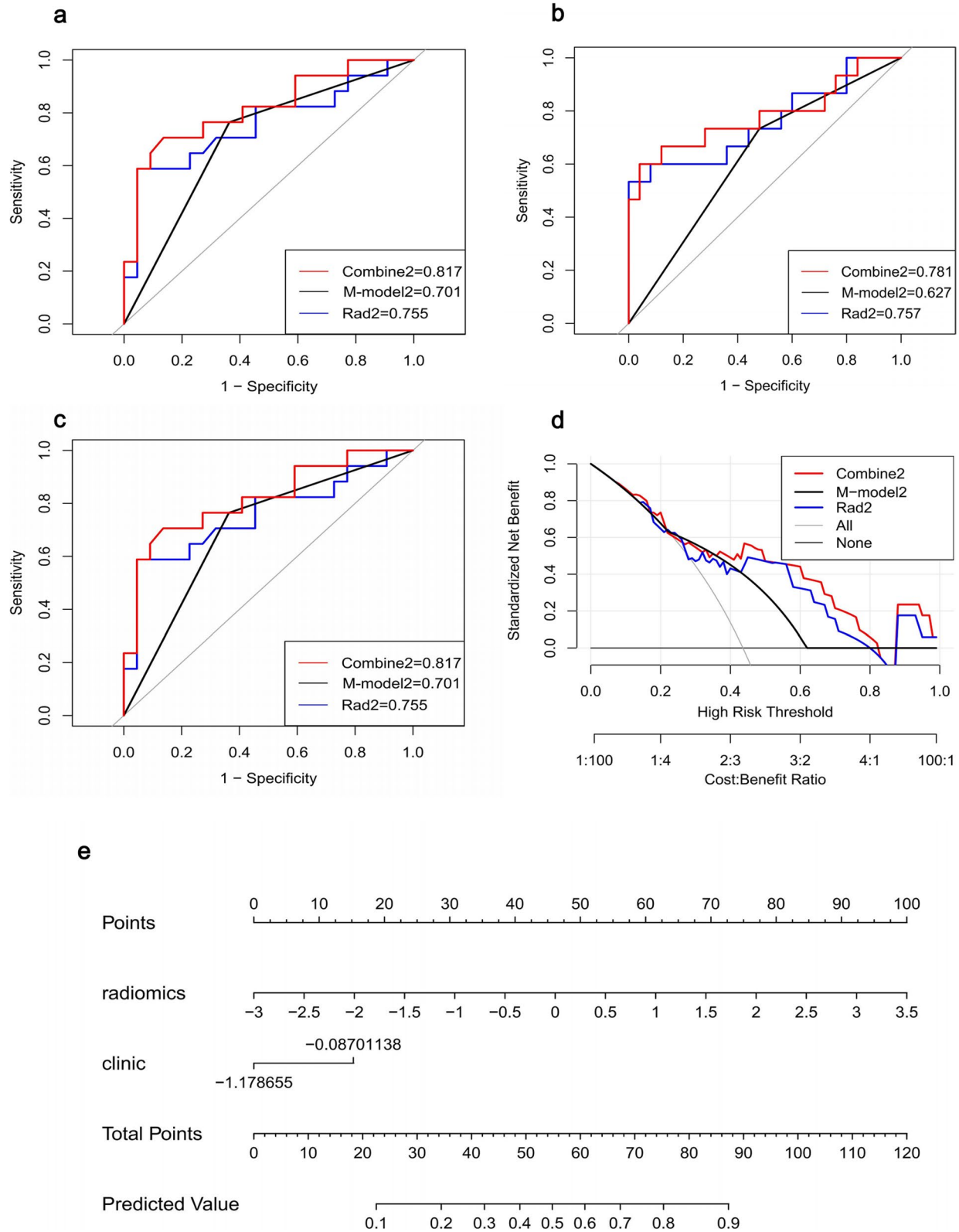

Fig. 4 The output of three models in distinguishing mild from moderate-to-severe activity (**a**-**b**) ROC of combine-model, radiomics-model, and morphology model in the training and testing cohort. **c** Calibration of three models in the testing cohort. **d** Decision curve analysis (DCA) of three models in the testing cohort. **e** Nomogram constructed by morphology radiomics combined model

Table 4 Performance of models for distinguishing mild from moderate-to-severe activity

models	Training cohort				Testing cohort			
	AUC (95%CI)	Accuracy	Sensitivity	Specificity	AUC (95%CI)	Accuracy	Sensitivity	Specificity
M-score2	0.701(0.554–0.847)	0.692	0.765	0.636	0.627(0.474–0.780)	0.600	0.733	0.520
Rad-score2	0.755(0.590–0.921)	0.795	0.588	0.955	0.757(0.585–0.930)	0.825	0.533	1.000
Combine-model2	0.817(0.676–0.958)	0.795	0.706	0.864	0.781(0.611–0.951)	0.825	0.600	0.960

Table 5 The comparison among the three different models

	Active vs. inactive		Mild vs. moderate-to-severe	
	Training cohort	Testing cohort	Training cohort	Testing cohort
M-score versus combine	0.002[a]	0.028[a]	0.040[a]	0.033[a]
Rad versus combine	0.001[a]	0.841	0.042[a]	0.055
Rad versus M-score	0.755	0.171	0.631	0.647

[a] Delong test

indicated that stenosis and comb sign were significantly correlated. Stenosis is the most often seen in patients with active inflammation, although fibrosis and inflammation are often both present [15]. Comb sign results from increased blood supply and drainage of a small bowel segment [23]. Wu et al. [24] reported that quantitative comb sign was effective in predicting CD activity, achieving an accuracy of 80% at the venous phase. A simplified CT enterography index of activity combined with mural thickness, mural stratification, and comb sign demonstrated a high and significant correlation with CD activity [25], with an AUC of 0.901. Our combined model surpassed this with an AUC of 0.944. In addition, Lopes et al. [26] found that endoscopic remission at 1-year follow-up was significantly correlated with improvements in mural hyperenhancement, mesenteric fat densification, comb sign, and strictures observed in CTE. These results further validated the robustness of our morphological models.

Our radiomics model included these features: original-firstorder-Median, wavelet-LLL-firstorder-Energy, wavelet-HLL-glszm-SizeZoneNonUniformity. "Median" represents the median gray level intensity within the ROI. Previous studies confirmed that the mean normalized iodine density was highly sensitive and specific for endoscopic active inflammation in CD patients [27, 28]. It suggested that the gray level intensity was related to the activity of the disease, which was consistent with our results. The two other features were Wavelet-filter features. Prior research concluded that Wavelet-filter features revealed the heterogeneity of ROI and suggested a poor prognosis [29]. Ding et al. [13] also reported that an MR radiomics model, which included five Wavelet-filter features, could evaluate the inflammatory severity and was comparable to MaRIA evaluated by a senior radiologist. Similar to other radiomics studies [30–32], we constructed the nomogram by combining both morphological and radiomics features, achieving the best predictive ability in both training and testing cohorts.

To the best of our knowledge, few studies have developed a radiomics model based on CTE imaging for assessing the disease activity. This preliminary study demonstrated that radiomics based on CTE could predict the inflammatory activity for ileocolonic CD, together with the morphological features could increase the accuracy of evaluation by radiologists. Furthermore, the segment-to-segment research method offered a more precise evaluation and could provide detailed information about each bowel segment to clinicians, allowing for more tailored treatment for patients.

It should be recognized that our study had several limitations. Firstly, this study was a retrospective study with a small sample size, which highlights the need for prospective research involving more patients from multiple centers to validate these findings. Secondly, we must acknowledge that CTE causes more radiation exposure to CD patients compared with MRE and ultrasonography, and more severely may lead to radiation-induced cancer. However, due to its high spatial and temporal resolution, few artifacts, and objective images, CTE remains wildly used in clinical practice. It is crucial to optimize imaging methods to minimize radiation exposure while maximizing the effectiveness of each CTE examination. Finally, we employed manual segmentation, which was time-consuming and

labor-intensive. Therefore, it is essential to develop a high-throughput method for automatic segmentation of medical images in the future.

In conclusion, we developed a combined model based on CTE radiomics and morphological features to differentiate the disease activity. The nomograms demonstrated satisfactory clinical utility in distinguishing disease activity in patients with CD.

Abbreviations

3D	Three-dimensional
AUC	Area under the ROC curve
CD	Crohn's Disease
CTE	Computed tomography enterography
DCA	Decision curve analysis
ROC	Receiver operating characteristic
VOI	Volume of interest
SES-CD	Simple endoscopic score for Crohn's disease
CRP	C-reactive protein
ESR	erythrocyte sedimentation rate
HBI	Harvey-Bradshaw

Acknowledgements
No.

Authors' contributions
Yuping Ma: Data curation, Software, Writing-original draft. Luanxin Zhu: Data curation, Software, Writing-original draft. Bota Cui: Data curation. Faming Zhang: Data curation. Writing-review & editing. Haige Li: Validation, Visualization. Jianguo Zhu: Conceptualization, Formal analysis, Methodology, Resources, Project administration, Supervision, Writing-review & editing. All authors read and approved the final manuscript.

Funding
The authors state that this work has not received any funding.

Data availability
All datasets and materials used and/or analyzed during the current study are available from the corresponding authors on any reasonable request.

Declarations

Ethics approval and consent to participate
The studies involving human participants were reviewed and approved by the Institutional Review Board and Ethics Committee of the Second Affiliated Hospital of Nanjing Medical University (ethical approval number: 2013KY034). Due to the retrospective nature of the current study, the Ethics Committee of the Second Affiliated Hospital of Nanjing Medical University waived the requirement for written informed consent from each participant. We confirm that all methods were carried out in accordance with relevant guidelines and regulations.

Consent for publication
Not applicable.

Competing interests
The authors declare no competing interests.

Author details
[1]Department of Radiology, the Second Affiliated Hospital of Nanjing Medical University, No. 121, Jiangjiayuan Road, Nan Jing 210011, P.R. China. [2]School of Stomatology, Xuzhou Medical University, Xu Zhou, P.R. China. [3]Department of Gastroenterology, the Second Affiliated Hospital of Nanjing Medical University, Nan Jing, P.R. China.

Received: 23 May 2024 Accepted: 14 January 2025
Published online: 27 January 2025

References

1. Ng SC, Shi HY, Hamidi N, Underwood FE, Tang W, Benchimol EI, Panaccione R, Ghosh S, Wu JC, Chan FK. Worldwide incidence and prevalence of inflammatory bowel disease in the 21st century: a systematic review of population-based studies. Lancet. 2017;390(10114):2769–78.
2. Maaser C, Sturm A, Vavricka SR, Kucharzik T, Fiorino G, Annese V, Calabrese E, Baumgart DC, Bettenworth D, Borralho Nunes P. ECCO-ESGAR Guideline for Diagnostic Assessment in IBD Part 1: initial diagnosis, monitoring of known IBD, detection of complications. J Crohn's Colitis. 2019;13(2):144–K164.
3. Sturm A, Maaser C, Calabrese E, Annese V, Fiorino G, Kucharzik T, Vavricka SR, Verstockt B, van Rheenen P, Tolan D. ECCO-ESGAR Guideline for Diagnostic Assessment in IBD Part 2: IBD scores and general principles and technical aspects. J Crohn's Colitis. 2019;13(3):273–84.
4. Mao L, Li Y, Cui B, Lu L, Dou W, Pylypenko D, Zhu J, Li H. Multiparametric MRI for Staging of Bowel Inflammatory Activity in Crohn's Disease with MUSE-IVIM and DCE-MRI: A Preliminary Study. Acad Radiol. 2024;31(3):880–8.
5. Zhu J, Zhang F, Zhou J, Li H. Assessment of therapeutic response in Crohn's disease using quantitative dynamic contrast enhanced MRI (DCE-MRI) parameters: A preliminary study. Medicine. 2017;96(32):e7759.
6. Zhu J, Zhang F, Luan Y, Cao P, Liu F, He W, Wang D. Can Dynamic Contrast-Enhanced MRI (DCE-MRI) and Diffusion-Weighted MRI (DW-MRI) Evaluate Inflammation Disease: A Preliminary Study of Crohn's Disease. Medicine (Baltimore). 2016;95(14):e3239.
7. Fernandes SR, Rodrigues RV, Bernardo S, Cortez-Pinto J, Rosa I, da Silva JP, Gonçalves AR, Valente A, Baldaia C, Santos PM. Transmural healing is associated with improved long-term outcomes of patients with Crohn's disease. Inflamm Bowel Dis. 2017;23(8):1403–9.
8. Chavoshi M, Mirshahvalad SA, Kasaeian A, Djalalinia S, Kolahdoozan S, Radmard AR. Diagnostic accuracy of magnetic resonance enterography in the evaluation of colonic abnormalities in Crohn's disease: a systematic review and meta-analysis. Acad Radiol. 2021;28:S192-202.
9. Dolinger M, Torres J, Vermeire S. Crohn's disease. Lancet. 2024;403(10432):1177–91.
10. de Sousa HT, Brito J, Magro F. New cross-sectional imaging in IBD. Curr Opin Gastroenterol. 2018;34(4):194–207.
11. Gao Y, Zhang B, Zhao D, Li S, Rong C, Sun M, Wu X. Automatic Segmentation and Radiomics for Identification and Activity Assessment of CTE Lesions in Crohn's Disease. Inflamm Bowel Dis. 2024;30(11):1957–64.
12. Lambin P, Rios-Velazquez E, Leijenaar R, Carvalho S, Van Stiphout RG, Granton P, Zegers CM, Gillies R, Boellard R, Dekker A. Radiomics: extracting more information from medical images using advanced feature analysis. Eur J Cancer. 2012;48(4):441–6.
13. Ding H, Li J, Jiang K, Gao C, Lu L, Zhang H, Chen H, Gao X, Zhou K, Sun Z. Assessing the inflammatory severity of the terminal ileum in Crohn disease using radiomics based on MRI. BMC Med Imaging. 2022;22(1):118.
14. Liu RX, Li H, Towbin AJ, Ata NA, Smith EA, Tkach JA, Denson LA, He L, Dillman JR. Machine learning diagnosis of small-bowel Crohn disease using T2-weighted MRI radiomic and clinical data. Am J Roentgenol. 2024;222(1):e2329812.
15. Magalhães FC, Lima EM, Carpentieri-Primo P, Barreto MM, Rodrigues RS, Parente DB. Crohn's disease: review and standardization of nomenclature. Radiologia Brasileira. 2023;56:95–101.
16. Zhu C, Hu J, Wang X, Li C, Gao Y, Li J, Ge Y, Wu X. A novel clinical radiomics nomogram at baseline to predict mucosal healing in Crohn's disease patients treated with infliximab. Eur Radiol. 2022;32(10):6628–36.
17. Li X, Zhang N, Hu C, Lin Y, Li J, Li Z, Cui E, Shi L, Zhuang X, Li J. CT-based radiomics signature of visceral adipose tissue for prediction of disease progression in patients with Crohn's disease: A multicentre cohort study. EClinicalMedicine. 2023;56:56.
18. Ruiqing L, Jing Y, Shunli L, Jia K, Zhibo W, Hongping Z, Keyu R, Xiaoming Z, Zhiming W, Weiming Z. A Novel Radiomics Model Integrating Luminal and Mesenteric Features to Predict Mucosal Activity and Surgery Risk in Crohn's Disease Patients: A Multicenter Study. Academic Radiology. 2023;30:S207-19.
19. Zhang R-n, Huang S-y, Liu R-y, Meng J-x, Zhou J, Chen Z, Fang J-y, Mao R, Li Z-p. Sun C-h: preoperative computed tomography enterography-based radiomics signature: a potential predictor of postoperative anastomotic recurrence in patients with Crohn's disease. Eur J Radiol. 2023;162:110766.

20. Tibshirani R. The lasso method for variable selection in the Cox model. Stat Med. 1997;16(4):385–95.
21. Daperno M, D'Haens G, Van Assche G, Baert F, Bulois P, Maunoury V, Sostegni R, Rocca R, Pera A, Gevers A. Development and validation of a new, simplified endoscopic activity score for Crohn's disease: the SES-CD. Gastrointest Endosc. 2004;60(4):505–12.
22. Meral M, Bengi G, Kayahan H, Akarsu M, Soytürk M, Topalak Ö, Akpinar H, Sagol Ö. Is ileocecal valve intubation essential for routine colonoscopic examination? Eur J Gastroenterol Hepatol. 2018;30(4):432–7.
23. Meyers M, McGuire P. Spiral CT demonstration of hypervascularity in Crohn disease:vascular jejunization of the ileum or the comb sign. Abdom Imaging. 1995;20:327–32.
24. Wu Y-W, Tao X-F, Tang Y-H, Hao N-X, Miao F. Quantitative measures of comb sign in Crohn's disease: correlation with disease activity and laboratory indications. Abdom Imaging. 2012;37:350–8.
25. Tong J, Feng Q, Zhang C, Xu X, Ran Z. CT enterography for evaluation of disease activity in patients with ileocolonic Crohn's disease. BMC Gastroenterol. 2022;22(1):1–10.
26. Lopes S, Andrade P, Afonso J, Cunha R, Rodrigues-Pinto E, Ramos I, Macedo G, Magro F. Monitoring Crohn's disease activity: endoscopy, fecal markers and computed tomography enterography. Therapeutic Adv Gastroenterol. 2018;11:1756284818769075.
27. Dane B, Kernizan A, O'Donnell T, Petrocelli R, Rabbenou W, Bhattacharya S, Chang S, Megibow A. Crohn's disease active inflammation assessment with iodine density from dual-energy CT enterography: comparison with endoscopy and conventional interpretation. Abdom Radiol. 2022;47(10):3406–13.
28. Dane B, Sarkar S, Nazarian M, Galitzer H, O'Donnell T, Remzi F, Chang S, Megibow A. Crohn disease active inflammation assessment with iodine density from dual-energy CT enterography: comparison with histopathologic analysis. Radiology. 2021;301(1):144–51.
29. Depeursinge A, Foncubierta-Rodriguez A, Van De Ville D, Müller H. Three-dimensional solid texture analysis in biomedical imaging: review and opportunities. Med Image Anal. 2014;18(1):176–96.
30. Bao D, Zhao Y, Li L, Lin M, Zhu Z, Yuan M, Zhong H, Xu H, Zhao X, Luo D. A MRI-based radiomics model predicting radiation-induced temporal lobe injury in nasopharyngeal carcinoma. Eur Radiol. 2022;32(10):6910–21.
31. Zhang Y, Liu L, Zhang K, Su R, Jia H, Qian L, Dong J. Nomograms combining clinical and imaging parameters to predict recurrence and disease-free survival after concurrent chemoradiotherapy in patients with locally advanced cervical cancer. Acad Radiol. 2023;30(3):499–508.
32. Zheng R, Zhang X, Liu B, Zhang Y, Shen H, Xie X, Li S, Huang G. Comparison of non-radiomics imaging features and radiomics models based on contrast-enhanced ultrasound and Gd-EOB-DTPA-enhanced MRI for predicting microvascular invasion in hepatocellular carcinoma within 5 cm. Eur Radiol. 2023;33:6462–72. https://doi.org/10.1007/s00330-023-09789-5.

Publisher's Note